Quantitative Perfusion Imaging with Total-Body PET

Juhani Knuuti[1,2], Jouni Tuisku[1], Henri Kärpijoki[1], Hidehiro Iida[1], Teemu Maaniitty[1,2], Aino Latva-Rasku[1], Vesa Oikonen[1], Sergey V. Nesterov[1], Jarmo Teuho[1], Maria K. Jaakkola[1], Riku Klén[1], Heli Louhi[1], Virva Saunavaara[1], Pirjo Nuutila[1], Antti Saraste[1,3], Juha Rinne[1], and Lauri Nummenmaa[1]

[1]Turku PET Centre, Turku University Hospital and University of Turku, Turku, Finland; [2]Department of Clinical Physiology, Nuclear Medicine, and PET, Turku University Hospital, Turku, Finland; and [3]Heart Center, Turku University Hospital and University of Turku, Turku, Finland

Recently, PET systems with a long axial field of view have become the current state of the art. Total-body PET scanners enable unique possibilities for scientific research and clinical diagnostics, but this new technology also raises numerous challenges. A key advantage of total-body imaging is that having all the organs in the field of view allows studying biologic interaction of all organs simultaneously. One of the new, promising imaging techniques is total-body quantitative perfusion imaging. Currently, ^{15}O-labeled water provides a feasible option for quantitation of tissue perfusion at the total-body level. This review summarizes the status of the methodology and the analysis and provides examples of preliminary findings on applications of quantitative parametric perfusion images for research and clinical work. We also describe the opportunities and challenges arising from moving from single-organ studies to modeling of a multisystem approach with total-body PET, and we discuss future directions for total-body imaging.

Key Words: PET/CT; radiotracer tissue kinetics; PET; perfusion; quantitation; total-body imaging

J Nucl Med 2023; 64:11S–19S
DOI: 10.2967/jnumed.122.264870

Until today, PET scanners have had a limited scanning area, with approximately 90% of the body outside the field of view (FOV), yielding no signal (*1*). Consequently, it has not been possible to simultaneously study interactions between organs and whole-body effects of interventions. Recently, PET/CT systems with a long axial FOV, such as the Biograph Vision Quadra (Siemens Healthineers) and the uEXPLORER (United Imaging), have become the state of the art. These new camera systems provide wider (>1 m) anatomic coverage and a significant increase in counting statistics and system sensitivity. The total-body PET scanners enable unique possibilities for scientific research but also for clinical diagnostics (*2–7*), but this new technology also raises numerous challenges (*8–11*).

A key advantage of total-body imaging is that having all the organs in the FOV allows studying biologic interaction of all organs simultaneously using a whole-body dynamic scan. For example, when performing cardiac scans, one can measure network-level interactions between the brain, heart, cardiovascular system, liver, pancreas, bowel, and muscles noninvasively. Higher sensitivity allows detecting fast-acting changes. Additionally, in most studies arterial or venous catheterization and blood sampling for tracer input calculation can be avoided because the input function can be obtained from the left ventricular cavity or the aorta.

In this paper, we describe one promising total-body PET imaging target: quantitative perfusion imaging from the perspective of our multidisciplinary total-body PET research team. We discuss the current state of total-body imaging and the advantages of the total-body approach for different imaging targets and clinical questions. We then describe the technical challenges and solutions of quantitative parametric perfusion imaging. Finally, with case examples we discuss the opportunities and challenges arising from moving from single-organ studies to modeling of a multisystem biology approach with total-body PET.

TOTAL-BODY PERFUSION WITH ^{15}O-WATER PET

Although there are reports demonstrating the feasibility of measuring blood flow with different perfusion tracers in specific organs such as ^{82}Rb (*12–16*), ^{15}O-water has many unique properties that make it particularly suitable for studying perfusion at the whole-body level. The other cardiac tracers have specific limitations that need to be overcome if used outside the heart as the target organ. Tracer extraction may not be ideal and may be nonlinear to flow, and kinetics may depend on metabolism, which needs to be considered.

^{15}O-water is a unique tracer because of its biologically inert characteristics. Its kinetics do not reflect chemical binding or metabolic processes. ^{15}O-water is also freely diffusible across the capillary membrane when passing through the capillary bed and is exchangeable with all tissue water molecules. The chemically inert characteristics of ^{15}O-water also mean that the kinetics of this tracer are solely dependent on the perfusion in the body organs, whereas the areas under the curve are essentially equal to those in the arterial input function in any organs. Modeling of ^{15}O-water PET data is based on the 1-tissue-compartment model (*17*), related to the Fick principle describing the exchange of inert gas between blood and tissues, in addition to the assumption of instantaneous exchange of ^{15}O-water with all tissue water molecules. PET imaging with ^{15}O-water provides quantitative accuracy for a wide range of transiently changing radioactivity, which is reflected by tissue perfusion values with a dynamic range of 0.04 mL/min/g (e.g., the skeletal muscle at rest) to 6.0 mL/min/g (e.g., the myocardium during stress).

The short half-life of ^{15}O (~122 s) also provides numerous advantages for assessing perfusion. First, repeated PET imaging for detecting transient changes during a single examination is doable with reasonably short administration intervals. The radiation dose for the patient is

Received Jun. 21, 2023; revision accepted Oct. 4, 2023.
For correspondence or reprints, contact Juhani Knuuti (juhani.knuuti@utu.fi).
Published online Nov. 1, 2023.

considerably small (e.g., 0.39 mSv for administration of 350 MBq of ^{15}O-water), enabling a wide range of applications to radiation-sensitive subject populations, for example, pediatric research subjects, repeat examinations in follow-up studies, normal-physiology experiments, and screening of high-risk subjects for studies.

The introduction of the perfusable tissue fraction improves accuracy in the quantitation of absolute myocardial perfusion by compensating for the partial-volume effects attributed to myocardial wall motion and the limited spatial resolution relative to the thickness of the myocardial wall (*18*). This approach may also be applied to other organs that have small or thin structures, such as the small intestine and colon. The perfusable tissue fraction concept is applicable in detecting and quantitating the fractional mass of tissue that is water-perfusable in the infarcted myocardium (*19*,*20*). Perfusable tissue fraction and its related index could also be good markers in predicting postoperative wall motion recovery after coronary artery revascularization (*21*,*22*). The presence of diffuse fibrosis in idiopathic cardiomyopathy could also be detected (*23*). The approach of using perfusable tissue fraction to assess viability in several organs such as the kidney and liver is promising.

QUANTITATIVE TOTAL-BODY PERFUSION IMAGING APPLICATIONS

Dynamic quantitative imaging of myocardial perfusion is feasible already with conventional PET scanners with a limited axial FOV and has been part of clinical routine for many years (*24*). The main clinical indication for myocardial perfusion imaging is the detection of obstructive coronary artery disease (CAD) in patients with chest pain or equivalent symptoms. Conventional, nonquantitative myocardial perfusion imaging relies on the detection of relative regional differences in myocardial perfusion, whereas quantitative imaging enables the absolute measurement of myocardial blood flow and flow reserve, which provides improved characterization of the extent and severity of multivessel CAD (*16*,*25*–*27*). Furthermore, quantitative PET myocardial perfusion imaging can detect reduced perfusion due to microvascular dysfunction, which often coexists with obstructive CAD but can also be present in the absence of epicardial CAD (*28*).

Obstructive CAD shares the same pathophysiologic atherosclerotic process that may be present in, for example, arteries supplying the brain (i.e., cerebrovascular disease) or lower limbs (i.e., peripheral artery disease), and a significant fraction of patients with atherosclerotic cardiovascular disease has more than one organ system involved (*29*). Similarly, systemic risk factors such as diabetes may promote microvascular dysfunction not only in the heart but also in other organs, such as the brain, eyes, and kidneys (*30*). Furthermore, cardiovascular diseases involve complex bidirectional interactions between the heart and other organs, including the immune system (*31*), nervous system (*32*), kidneys (*33*), and endocrine system (*34*). For example, cardiovascular diseases have effects on the nervous system whereas neurologic disorders may affect the cardiovascular system, sometimes called the heart–brain axis (*35*). Many cardiovascular therapies are also partly based on their effects outside the cardiovascular system, such as in the neurohormonal, endocrine, or immune system (*32*,*36*). These findings highlight the need to investigate the interplay of different organ systems, and total-body perfusion imaging provides one solution for this need.

Silent brain infarcts and cerebral hypoperfusion are associated with an increased risk of symptomatic stroke and dementia, and thus their detection in individuals with vascular disease in other parts of the body is important for preventive measures. Whole-body PET imaging could reveal silent brain infarcts or cerebral perfusion deficit in, for example, a subject with atherosclerosis imaged for other indications. The more specific nature of the deficit could be investigated with multimodal PET imaging addressing the cerebral metabolic rate of oxygen, oxygen extraction ratio, and cerebral blood volume together with MRI (*37*).

Higher mental processes and their neural bases are tightly linked with the internal homeostatic control of the body (*38*), and the brain responds continuously to the visceral, immunologic, metabolic, and sensorimotor signals (*39*). Integration of these afferent signals is used for altering bodily functions and driving complex motivated behaviors. The central–peripheral axis and particularly cardiorespiratory functions have emerged as a potential imaging target for affective disorders. For example, anxiety is common in patients with cardiovascular diseases (*40*,*41*)—not just because of the fear of cardiac disease but because of altered integration of the central–peripheral emotion circuits. Conversely, anxiety is recognized as an independent risk factor for cardiovascular disease due to an emotion-induced increase in cardiorespiratory tone (*42*,*43*), and resting-state amygdala activity and concomitant anxiety are associated with increased risk for cardiovascular disease events and arterial inflammation (*44*). Nevertheless, systems-level understanding of the crosstalk of the central–peripheral circuits in anxiety and cardiovascular disease remains elusive, and the systemic crosstalk between the brain and the peripheral organs during acute emotions and prolonged perturbations of the emotion circuit remain poorly understood. Total-body PET imaging can potentially transform human systems neuroimaging by shifting the focus from dualistic studies on the brain and periphery to high-resolution activation imaging across the brain and peripheral organs, creating an innovative new multisystem-biology approach for studying the central and peripheral bases of higher mental processes and their dysfunctions.

Alteration in tissue perfusion is also characteristic of metabolic syndrome, and therefore the cellular- and tissue-level mechanisms contributing to the coincidence of cardiovascular disease and insulin resistance continue to be a target of intense research. One line of research has shown that in obesity, insulin resistance, and type 2 diabetes, the vasodilatory effect of insulin is impaired, with insulin resistance thought to associate with endothelial dysfunction. With the novel scanners it has now finally become possible to assess changes in tissue blood flow and the distribution of blood flow occurring in metabolic syndrome and to clarify the interactions between downregulated tissue metabolism and blood flow (*45*–*48*).

There are a number of other potential research applications for total-body perfusion PET imaging, but these details are beyond this review. Tumor and metastasis perfusion could help in detecting cancer tissues because perfusion is typically increased in cancer (*49*) and could be a useful imaging marker for predicting treatment responses (*50*,*51*). The heart–kidney connection appears to be important in various conditions and diseases. For example, in the cardiorenal syndrome, the altered function of the heart and the kidneys is linked to regulation of the sympathetic nervous system (*52*).

TECHNICAL CHALLENGES AND SOLUTIONS OF WHOLE-BODY ^{15}O-WATER PET IMAGING

Tracer Dose

High sensitivity achieved by total-body PET/CT is of value in improving image quality or lowering injected dose. Image quality is known to be worsened when the ^{15}O-water injection dose is low

because of a lack of count statistics in the PET images. On the other hand, image quality is degraded if the injection dose is too high, attributed to the increased random rates causing increased noise and systematic errors. We have tested the performance of the Quadra scanner with various ^{15}O-water doses (from 20 to 700 MBq) to understand the performance and limitations of the scanner and to define the image acquisition protocol that can provide reasonable image quality with maintained quantitative accuracy. Our preliminary results suggest that the largest injected dose for optimal image quality is 700 MBq, with no systematic errors on quantitative perfusion being present. On the basis of these results, we have been using an injected dose of 350–400 MBq in ongoing clinical projects.

Automated Production and Injection Control

If very high radioactivity is present in the infusion catheter and in the arm when the injected radioactivity reaches the left ventricle and other organs, there could be problems due to counting rate limitations because the infusion tube has a very weak attenuation. A dedicated ^{15}O-water delivery system (Hidex) was therefore programmed to flush the tracer by saline and minimize the period when high radioactivity is in the catheter, allowing most radioactivity to reach the circulation very quickly. Because of strong attenuation, the total count rate reduces to a reasonable level when tracer is distributed to the body. Automated tracer delivery control is important for reproducibility.

Image Acquisition

List-mode acquisition in total-body studies yields large datasets whose analysis is computationally prohibitive. A typical list-mode raw data file after a 4-min 40-s scan with 350 MBq of ^{15}O-water with a Siemens Vision Quadra is 25 Gb. Although raw data can be archived, in practice the predefined dynamic reconstruction to, for example, 24 frames (14×5 s, 3×10 s, 3×20 s, and 4×30 s) is performed with a reconstructed voxel size of $1.65 \times 1.65 \times 2.8$ mm.

Extending PET imaging time with ^{15}O-water does not improve the count statistics, particularly in organs that have high flow. Instead, injected dose and administration duration are the parameters that maximize PET image quality, as long as the counting rate performance of the PET device is not exceeded. Because of the wide range of tissue flow values, high counting rate performance and high sensitivity are essential requirements for simultaneous quantitation of total-body tissue perfusion.

Currently, the reconstruction of dynamic images with a matrix size of $440 \times 440 \times 380$ and 24 frames takes 35 min. The single-image file size is 383 kb and the total series is 3.33 Gb, which can be handled with current image analysis software such as Carimas (Turku PET Centre). Quantitation of perfusion in high-flow tissues such as the heart is feasible also with shorter acquisition times (*53*), but for tissues with a lower flow, a longer scan duration such as explained above is warranted. In addition, the sensitivity profile of the scanner is uneven, depending on the scanning mode. To achieve maximum sensitivity, the brain should not be positioned at the edge of the FOV because sensitivity decreases toward the edges. Figure 1 shows the simulated time–activity curves of tissues with variable flow levels.

Mathematic Model for Quantitation

A single-tissue-compartment model that includes the water-perfusable tissue fraction and the arterial blood component is an out-of-the-box solution for modeling most organs with ^{15}O-water PET. However, a unified fitting solution for kinetic modeling of all organs requires additional work. For example, in the lungs and liver, two input functions are needed. The pulmonary artery carries a large volume of blood (*54*) whereas the blood supply to the bronchioles through the bronchial artery is much smaller, although oxygen and substrates are carried to the bronchioles under normal physiologic conditions. Lung tumors have been considered perfused by the pulmonary artery system (*55*). In the liver, the portal vein carries a higher volume of blood than the hepatic artery. One potential solution for modeling of liver perfusion involves estimation of portal vein input function from the measured hepatic arterial input function and liver time–activity curves based on mathematic modeling (*56*). Although there are several works on lung (*57*) and liver (*56*,*58*) perfusion, the detection of input function from the bronchial artery and the portal vein has been difficult in previous PET scanners. This might be more feasible with total-body PET scanners, which provide better spatial resolution and higher accuracy in measuring a wide range of perfusion levels. Further careful investigation is needed to investigate the potential impacts in case the fundamental assumptions that we applied, such as the instantaneous equilibrium, exchangeability of ^{15}O-water to tissue water, homogeneity in the flow distribution, and no arterial-to-venous shunt, may be limited in some organs. Organ-specific optimization of the model with careful validation is warranted to provide physiologically verified reliable and disease-sensitive tissue perfusion values.

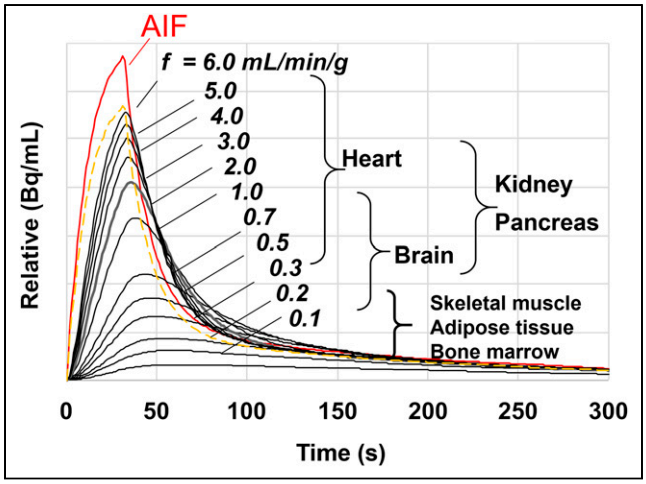

FIGURE 1. Simulated tissue time–activity curves (black lines) and arterial input function (red line) of dynamic ^{15}O-water scans. AIF = aorta input function curve; f = flow.

Patient Motion Prevention and Compensation

Patient motion is a challenge for total-body PET systems because body and limb movements have multiple degrees of freedom. Since the entire body is within the imaging FOV at all times, any changes in the patient's position can result in blurring or issues with attenuation correction and region-of-interest delineation. Comfortable positioning of the patient, limb supports, and head fixation are important means for prospective motion prevention.

One solution to cyclic motion detection is deviceless gating. Advanced reconstruction methods can also address this problem, although reconstruction times may be significantly extended. Motion compensation and tracking in PET systems with a short axial FOV have been concentrated to tracking and correction for cardiac and respiratory motion, as well as their combination. However, motion patterns in PET systems with a long axial FOV are more complex,

consisting of complex body motions; subtle motions such as swallowing, nodding, or head bobbing; and peristaltic, cardiac, and respiratory motions. This requires more refined methods in addition to traditionally applied motion correction methods and algorithms, whereas diffeomorphic registration and deep learning–based methods have been applied successfully so far (*59*,*60*).

Whereas several tracking solutions have been developed to account for cardiac and respiratory motion, only proof-of-concept methods using optical tracking have been applied so far to track body motion in total-body PET imaging. Thus, there is a need to assess both tracking devices and PET data–based methods to derive motion signals as well as compensation methods applicable to PET systems with a long axial FOV. Because of increased sensitivity, dynamic PET reconstructions with even a subsecond duration are feasible, and novel motion correction approaches can be implemented by deriving motion signals from dynamic PET data alone. For example, changes and oscillations in the dynamic time–activity curves can be used to monitor changes due to respiratory and cardiac motion and to derive motion signals based on these oscillations (*1*). However, PET data–based methods might be more challenging to apply to tracers such as ^{15}O-water because of fast tracer kinetics.

Tissue Segmentation

An effective and automated segmentation method is a prerequisite for analysis for the large amount of complex data a total-body system produces. Especially, dynamic images with temporal information and PET images with short–half-life traces, such as water, are challenging to segment manually, as this would lead to a significant workload and operator-dependent variability. Therefore, fully automated methods for delineation and analysis of organs, as well as smaller targets such as ischemic lesions, are required.

The state-of-the-art segmentation methods for ^{15}O-water PET imaging consist of the semiautomatic cardiac analysis pipeline, CT-based total-body segmentation, and clustering of total-body PET images. Semiautomatic cardiac segmentation of dynamic PET images involves user-defined markers to segment the myocardium for modeling (*61*), but this approach does not generalize to the other parts of the image. Fully automated CT-based total-body segmentation algorithms, such as TotalSegmentator (*62*) and MIWBAS (*63*), use deep neural networks trained on labeled data. Despite their accuracy, these methods are not yet able to segment all different tissue types or subparts of an organ, such as the medulla and cortex of the kidney. Another drawback in CT-based segmentation applied to PET images is that the anatomic information of CT does not entirely match the PET functional information. It is also apparent that CT and PET images should be coregistered to eliminate potential misalignment, and PET data would require frame-by-frame realignment for correcting subject motion.

Use of unsupervised clustering for PET time–activity curves enables new PET-based total-body segmentation methods applying the physiologic information. The disadvantage is that functional data clustering does not always produce clinically meaningful results, but this problem can be resolved by combining PET-based clustering with CT-based segmentation. An example of total-body CT- and PET-based segmentation is shown in Figure 2.

Determination of Arterial Input Function

A higher-quality input function is required for total-body PET examinations than for single-organ measurement, because of the higher range of perfusion values and more blood components in the tissues of some organs. Definition of the volume of interest to obtain the arterial input function is the first step in the postprocessing PET image analysis. The descending aortic artery is typically selected for detection of arterial input function because this location is near most organs. To that end, a single-line volume of interest with 1–2 pixels in each slice and 25–30 cm in length is defined manually. Patient movement can then be considered, and the volume-of-interest data can be corrected. To avoid labor-intensive work, a semiautomated technique is under development. This step must be well validated because of its importance for the quantitative analysis.

Correction for the delay and dispersion of the arterial input function in ^{15}O-water PET studies is also critical. In total-body PET with aortic arterial input function, the magnitude of the correction for delay and dispersion is much smaller than in the classic examinations that used peripheral blood sampling. Of note is that the dispersion-added input function has the same formulation as the tissue radioactivity curve, where arterial input function and the tissue curve are close to each other at a high-flow region. Theoretically, the vascular volume (the third parameter in the model formulation for ^{15}O-water) has the same interpretation as the dispersion time constant if one approximates the dispersion as the single exponential function (*64*). Delay could have similar effects. Obviously, a unique solution is required to determine the delay and dispersion in addition to the model parameter sets. The work of Wang et al. (*65*) also introduced an approach that defines the optimal model configuration for each voxel by means of the Akaike information criterion. A similar approach can be applied to ^{15}O-water examinations to identify the model configuration.

Analysis Framework

Large datasets covering multiple organs and tissues propose a major challenge for modeling total-body PET data. A universal voxelwise model cannot be applied across the image because of the variations in tracer uptake kinetics across organs. Thus, radiotracer delay and dispersion parameters would need to be adjusted regionally, and a priori regions of interest need to be delineated for tissue-specific modeling. Neither manual delineation of tens of different regions of interest per subject nor warping of the total-body images accurately into a common stereotactic space is feasible.

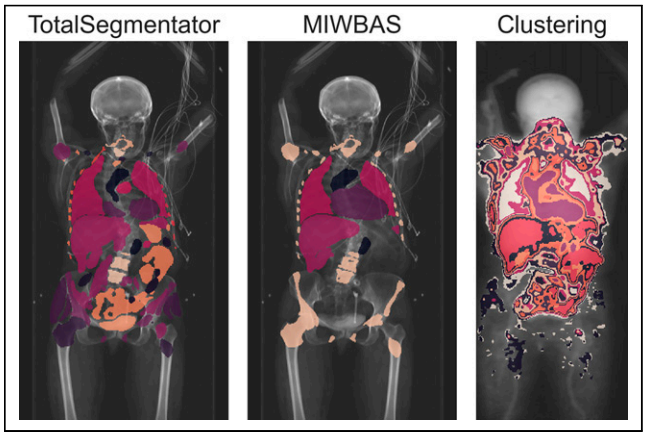

FIGURE 2. Example of automated tissue segmentation of total-body PET/CT images done with TotalSegmentator (CT-based), MIWBAS (CT-based), and clustering (PET-based). Segmentations at middle coronal slice are visualized with original CT or PET image (sum over coronal slices to flatten them into 2 dimensions) in background for reference. TotalSegmentator and MIWBAS segment their predefined volumes of interest, whereas clustering segments all areas that end user defines as foreground without annotating resulting segments.

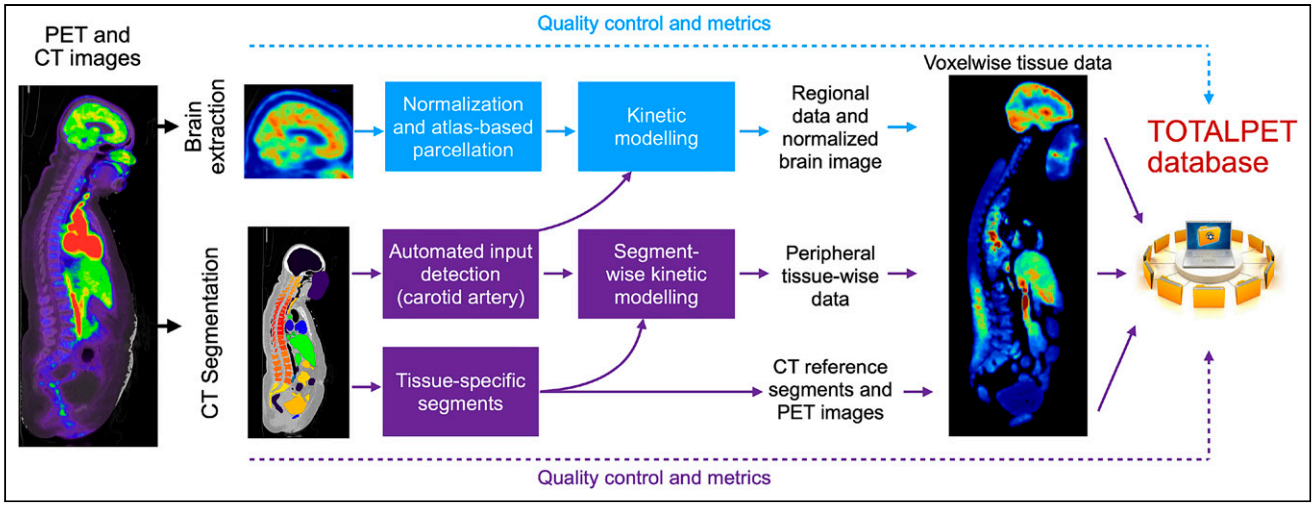

FIGURE 3. Developed framework for whole-body ^{15}O-water PET data processing and kinetic modeling. Validation of this framework is currently in progress. TOTALPET database denotes final image archive of parametric images.

For the reasons described above, we have been developing a novel modeling framework for fast, automated, and replicable analysis of total-body PET data. The pipeline uses openly available in-house software (http://www.turkupetcentre.net/petanalysis/) for whole-body and brain data analysis (*66*). The proposed method (Fig. 3) automates the PET data modeling by joint use of CT and PET images and time–activity curve information for the segmentation. CT-based segmentation (TotalSegmentator) of major organs and tissues is first run for generating tissue-type priors. Next, principal-component analysis–based segmentation on the voxelwise PET time–activity curves is generated for the PET data, whereas CT segmentation is used to restrict clustering within single organs. For brain, either CT- or PET-template–based normalization provides a way to map region-of-interest atlases, such as AAL3 (*67*) from MNI152 space to native PET space.

Consequently, a 1-tissue-compartment model is fitted for each segment both at the region-of-interest level and at the voxel level, accounting for the differences in radiotracer delay. This yields tissue-specific mean regional outcome values for statistical analysis (Fig. 4) and organ-specific parametric maps (Fig. 5). Our framework is flexible, allowing unique parametrization of each modeled organ, and thus it can also be readily adapted to model other radiotracers, such as [^{18}F]FDG.

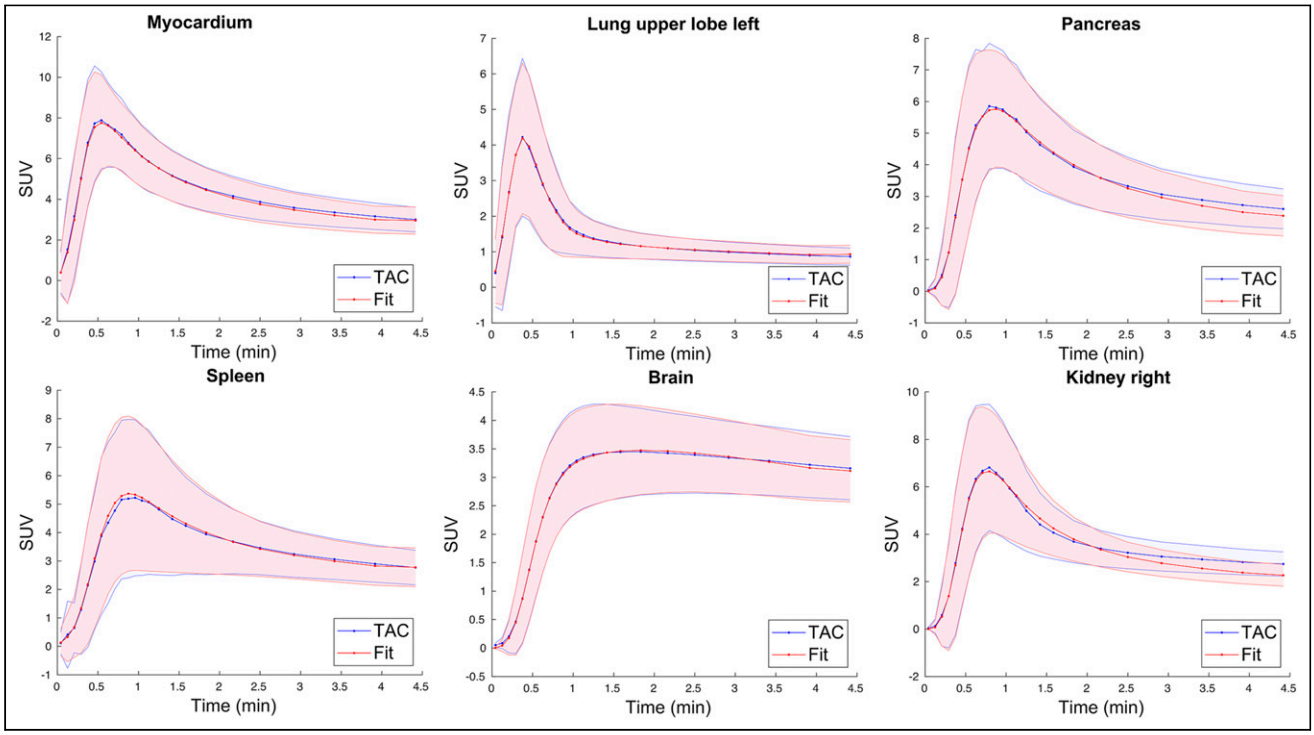

FIGURE 4. Mean ^{15}O-water different PET time–activity curves within volume-of-interest regions (red) and mean compartment model fits (blue) corresponding to automatically segmented organs. Shaded areas illustrate SD of data and corresponding model fits (means and SD calculated over analyzed studies [n = 93]).

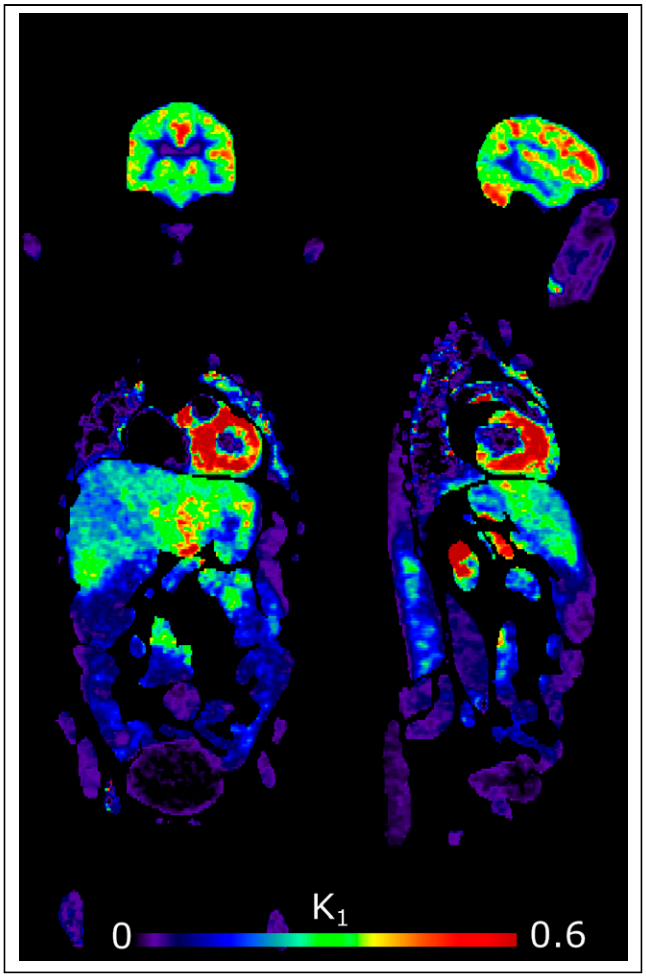

FIGURE 5. Quantitative parametric perfusion image with organ specific voxel level mathematic modeling that accounts for differences in radiotracer delay.

INITIAL EXPERIENCES WITH TOTAL-BODY QUANTITATIVE PERFUSION PET

Institutional Review Board

The institutional review board of the Welfare Services County of Southwest Finland has approved this study, and all study subjects signed a written informed consent form.

Dynamic Image Quality and Total-Body Parametric ^{15}O-Water Images

Figure 6 shows the dynamic sequence of early frames after injecting 350 MBq of ^{15}O-water. The 10-s bolus of ^{15}O-water in 20 mL was given using the specific delivery system (Hidex) with a flush of 10 mL. The visual image quality was good even with 5-s frame durations, with clear visualization of body organs.

The next step was to test the quality of the data and the stability of performing voxel-level fitting of the whole-body dynamic ^{15}O-water image set. The example in Figure 7 demonstrates that good-quality parametric images can be created using a single input function from the aorta and applying the same 1-tissue compartment model for each image voxel of the whole body (rotating videos are provided as Supplemental Video 1, available at http://jnm.snmjournals.org).

Clinical Cases and Preliminary Findings for Total-Body Perfusion Imaging

For nearly 20 y in our center, ^{15}O-water PET has been routinely used to quantify perfusion in absolute terms in the hearts of patients with suspected CAD. Since fall 2022, we have performed all clinical cardiac scans with a total-body scanner aiming to investigate the association of reduced myocardial perfusion with perfusion in other tissues such as the brain and kidneys. Our hypothesis is that obstructive CAD is linked with changes in perfusion in other organs and that these changes may also have clinical consequences. Figure 8 shows an example of a patient who underwent a clinically indicated cardiac ^{15}O-water PET scan because of suspected CAD. As the total-body perfusion was routinely performed, we were able to also study other organs of the body, including the brain. The patient demonstrated a clear perfusion deficit in the right parietooccipital area, and the brain infarction was subsequently confirmed with CT.

One current research question about the interaction of the brain–heart axis is the effect of anxiety on cardiac and cerebral integration. In this analysis, we benchmarked the automated segmentation and modeling tool (described above) for mapping interactions of the central and peripheral circuits in anxiety during adenosine-induced cardiac stress and at the resting baseline. Proof-of-concept results are shown in Figure 9. Self-reported bodily sensation maps indicate that adenosine evokes unpleasant bodily sensations (Fig. 9A) and that the experience of anxiety is associated with increased cerebral perfusion in key nodes of the limbic, paralimbic, and cortical emotion circuits (Fig. 9B). Interorgan regional correlations in perfusion are widespread during stress and become more focused during adenosine

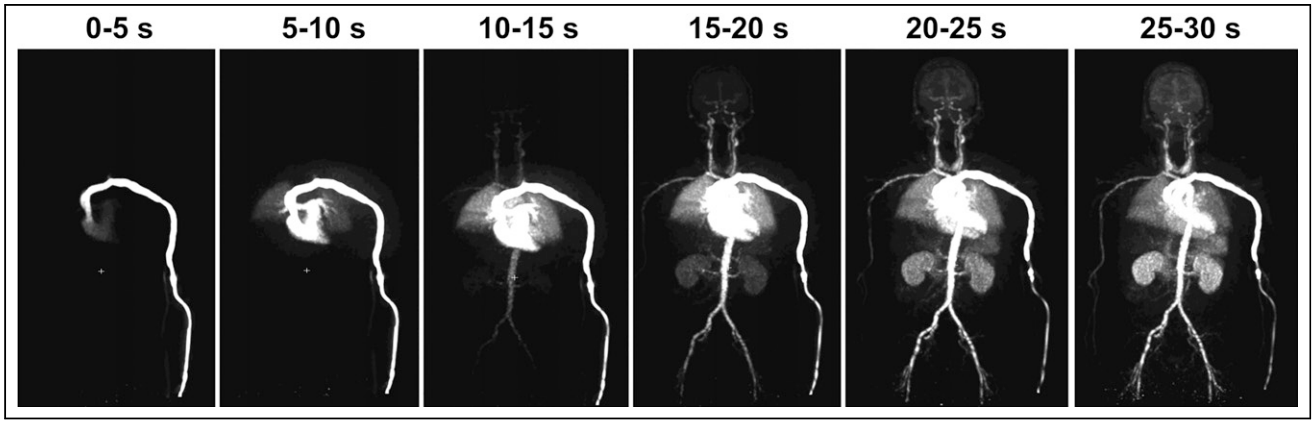

FIGURE 6. Dynamic 5-s images after ^{15}O-water injection of one of first patients.

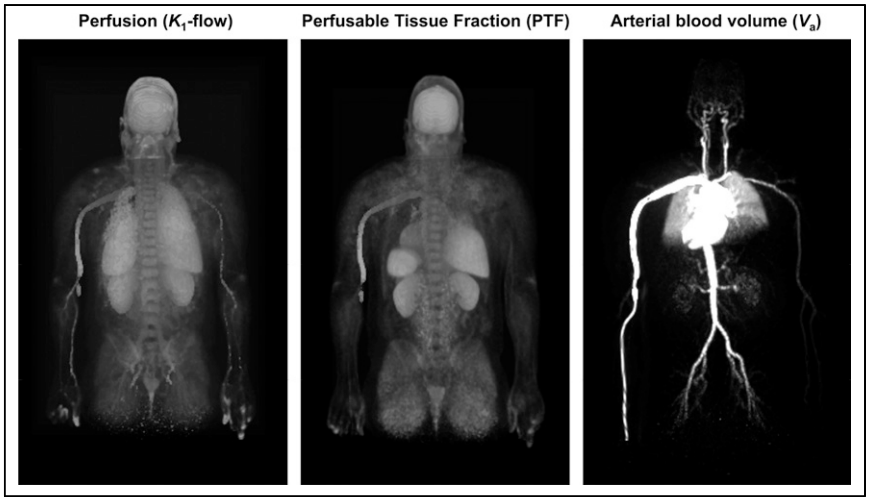

FIGURE 7. One of first cases of total-body parametric images with ^{15}O-water shown by Carimas software. Images are processed to three 3-dimensional parametric components: tissue perfusion, perfusable tissue fraction, and arterial blood volume images. Delay and dispersion corrections were not applied, and same model was used in all organs. Therefore, these parametric images are not yet ideal; for example, K_1 is influenced by arterial vessels largely attributed to delay and dispersion, and in heart, K_2-weighted model is applied.

infusion, indicating stronger integration during pharmacologic stress. These results provide the first-ever (to our knowledge) total-body quantification of the central and peripheral circuits during acute anxiety, paving the way for novel network-level studies on the central–peripheral distributed mechanism of higher mental processes.

FUTURE DEVELOPMENT OF TOTAL-BODY PERFUSION IMAGING

Calculation of parametric images can be expedited using the basis function method (*68*), in which the convolution integral is tabulated as a function of rate constant K_2, and the calculation could be parallelized. This is particularly important for the large datasets acquired with total-body PET. Use of a graphics processing unit can speed up the calculation even more, provided that the kinetic fitting programs are compatible with the unit specification. Several techniques established for cerebral blood flow imaging could also be extended to other organs in total-body data. Since the adequacy of the compartment model is not known in several organs, the graphic plot approach (*69*) is currently being evaluated to determine the K_1 flow without assuming any compartment model configurations and to test the adequacy of the compartmental assumptions. The weighted integral approach (*70*,*71*) could also be used as a fast alternative to standard nonlinear least-squares methodology when calculating parametric images.

Efficient data processing and storage solutions are still a work in progress. Currently, our approach involves a centralized computer cluster that includes multiple computer nodes with fast central and graphics processing units and large memories. These cluster nodes may run multiple processers for functional image calculation for each organ, each patient, and different model configurations.

Artificial intelligence solutions will likely further enhance image quality. For example, applying deep learning methods could enhance workflow and speed up computationally intensive tasks related to data analysis, image registration, or reconstruction using models with a relatively short inference time. Moreover, there are multiple applications in which deep learning can be applied: automated analysis, data enhancement via denoising or resolution improvement, estimation of dispersion or delay corrections, estimation of tracer kinetics directly in kinetic modeling, and effective performance of otherwise complex tasks such as motion correction (*72*).

The longer PET FOV also requires that total-body CT be performed for every subject on each examination, and this increases radiation dose. Even ultra-low-dose attenuation CT scans are currently available with less than a 0.5-mSv total radiation dose for the whole-body scan; alternative low-dose solutions are warranted, especially with pediatric studies. Among several approaches for CT-free attenuation correction, one is to create attenuation data using background γ-rays emitted from the lutetium oxyorthosilicate detector. A small amount of natural ^{176}Lu in the lutetium oxyorthosilicate scintillation detector emits γ-rays of 307, 202, and 88 keV simultaneously (half-life, 38×10^9 y) (*73*). Using a total-body PET scanner, a μ-map can be calculated with systematic errors of 5%–7% in the same way as for the transmission scan (*74*). The systematic errors could be reduced by applying machine learning even for postemission attenuation μ-imaging (*75*). It is of interest to develop a technique without the need for the machine learning approach, because training and validation data may be difficult to acquire with radiation to patients.

A unique application is the myocardial perfusion study, in which respiration-related periodic motion may not be present because of temporal smoothing over the entire transmission acquisition period. This could be used as a reference to evaluate and improve CT-based attenuation correction during respiratory motion.

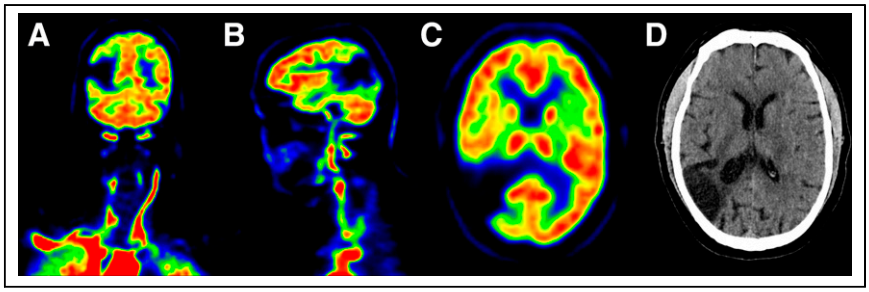

FIGURE 8. Brain infarction in parietooccipital watershed area detected by total-body perfusion PET: coronal PET slice (A), sagittal PET slice (B), transaxial PET slice (C), and transaxial corresponding CT image confirming brain infarction (D). Images are summed PET images of all frames of dynamic scan.

SUMMARY AND CONCLUSIONS

With new-generation extended-FOV PET/CT scanners, total-body quantitative perfusion imaging appears to have become a realistic possibility. ^{15}O-water as a biologically inert and freely diffusible tracer is likely the tracer of choice for perfusion quantitation. Preliminary experience has already shown that automated image

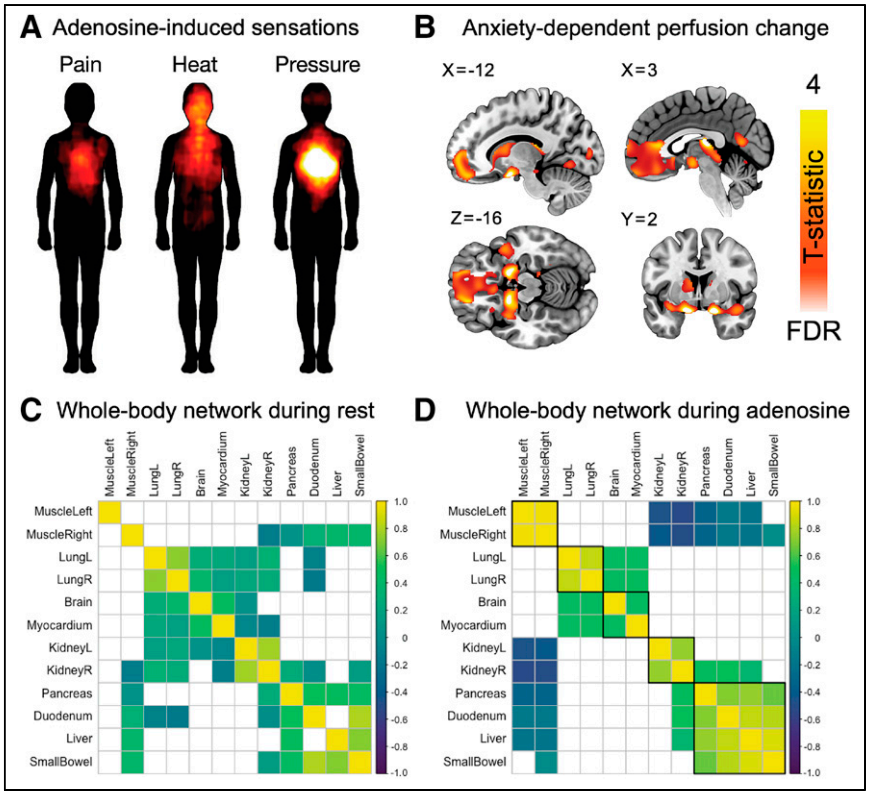

FIGURE 9. Proof-of concept results in patients with suspected CAD entering total-body perfusion PET. (A) Adenosine induces unpleasant bodily sensations. (B) Adenosine-induced anxiety is associated with increased perfusion in brain's emotion circuits. (C and D) Regional correlations in perfusion are widespread during rest (C) but become increasingly focused during adenosine-induced stress (D). FDR = false discovery rate.

segmentation and analysis appear feasible and promising. Currently, several technical and analysis solutions are still under development and warrant further research. However, it already appears that biologic interaction of all body organs could be studied noninvasively. This ability will open new avenues for research and clinical work and is likely to transform our understanding of the abnormalities of various diseases such as in obesity, diabetes, and cardiovascular diseases.

DISCLOSURE

The study was supported by grants from the Finnish Cultural Foundation, the Jane and Aatos Erkko Foundation, the Finnish Foundation for Cardiovascular Research, Sigrid Juselius stiftelse and Academy of Finland, and Finnish State Research Funding. Juhani Knuuti received consultancy fees from GE Healthcare and Synektik and speaker fees from GE Healthcare, Bayer, Lundbeck, Boehringer-Ingelheim, Pfizer, Siemens Healthineers, and Merck, outside the submitted work. Antti Saraste received consultancy fees from Amgen, Astra Zeneca, Boehringer Ingelheim, and Pfizer and speaker fees from Abbott, Astra Zeneca, and Bayer. No other potential conflict of interest relevant to this article was reported.

REFERENCES

1. Zhang X, Cherry SR, Xie Z, Shi H, Badawi RD, Qi J. Subsecond total-body imaging using ultrasensitive positron emission tomography. *Proc Natl Acad Sci USA.* 2020;117:2265–2267.
2. Rodriguez JA, Selvaraj S, Bravo PE. Potential cardiovascular applications of total-body PET imaging. *PET Clin.* 2021;16:129–136.
3. Saboury B, Morris MA, Farhadi F, et al. Reinventing molecular imaging with total-body PET, part i: technical revolution in evolution. *PET Clin.* 2020; 15:427–438.
4. Saboury B, Morris MA, Nikpanah M, Werner TJ, Jones EC, Alavi A. Reinventing molecular imaging with total-body PET, part II: clinical applications. *PET Clin.* 2020;15:463–475.
5. Sui X, Liu G, Hu P, et al. Total-body PET/computed tomography highlights in clinical practice: experiences from Zhongshan Hospital, Fudan University. *PET Clin.* 2021;16:9–14.
6. Slart RHJA, Tsoumpas C, Glaudemans AWJM, et al. Long axial field of view PET scanners: a road map to implementation and new possibilities. *Eur J Nucl Med Mol Imaging.* 2021;48:4236–4245.
7. van Sluis J, van Snick JH, Brouwers AH, et al. EARL compliance and imaging optimisation on the Biograph Vision Quadra PET/CT using phantom and clinical data. *Eur J Nucl Med Mol Imaging.* 2022;49:4652–4660.
8. Hicks RJ. So, you want to get into "total-body" PET/CT scanning? An installation guide for beginners! *Cancer Imaging.* 2023;23:35.
9. Hoffmann EJ, Phelps ME, Mullani NA, Higgins CS, Ter-Pogossian MM. Design and performance characteristics of a whole-body positron transaxial tomograph. *J Nucl Med.* 1976;17:493–502.
10. Badawi RD, Shi H, Hu P, et al. First human imaging studies with the EXPLORER total-body PET scanner. *J Nucl Med.* 2019;60:299–303.
11. Nardo L, Pantel AR. Oncologic applications of long axial field-of-view PET/computed tomography. *PET Clin.* 2021;16:65–73.
12. Langaa SS, Lauridsen TG, Mose FH, Fynbo CA, Theil J, Bech JN. Estimation of renal perfusion based on measurement of rubidium-82 clearance by PET/CT scanning in healthy subjects. *EJNMMI Phys.* 2021;8:43.
13. Tahari AK, Bravo PE, Rahmim A, Bengel FM, Szabo Z. Initial human experience with rubidium-82 renal PET/CT imaging. *J Med Imaging Radiat Oncol.* 2014;58:25–31.
14. Nitzsche EU, Choi Y, Killion D, et al. Quantification and parametric imaging of renal cortical blood flow in vivo based on Patlak graphical analysis. *Kidney Int.* 1993;44:985–996.
15. Mossberg KA, Mullani N, Gould KL, Taegtmeyer H. Skeletal muscle blood flow in vivo: detection with rubidium-82 and effects of glucose, insulin, and exercise. *J Nucl Med.* 1987;28:1155–1163.
16. Sciagrà R, Lubberink M, Hyafil F, et al. EANM procedural guidelines for PET/CT quantitative myocardial perfusion imaging. *Eur J Nucl Med Mol Imaging.* 2021;48: 1040–1069.
17. Kety SS, Schmidt CF. The nitrous oxide method for the quantitative determination of cerebral blood flow in man: theory, procedure and normal values. *J Clin Invest.* 1948;27:476–483.
18. Iida H, Kanno I, Takahashi A, et al. Measurement of absolute myocardial blood flow with $H_2{}^{15}O$ and dynamic positron-emission tomography. Strategy for quantification in relation to the partial-volume effect. *Circulation.* 1988;78:104–115.
19. Iida H, Tamura Y, Kitamura K, Bloomfield PM, Eberl S, Ono Y. Histochemical correlates of ^{15}O-water-perfusable tissue fraction in experimental canine studies of old myocardial infarction. *J Nucl Med.* 2000;41:1737–1745.
20. Iida H, Rhodes CG, De Silva R, et al. Myocardial tissue fraction: correction for partial volume effects and measure of tissue viability. *J Nucl Med.* 1991;32:2169–2175.
21. de Silva R, Yamamoto Y, Rhodes CG, et al. Preoperative prediction of the outcome of coronary revascularization using positron emission tomography. *Circulation.* 1992;86:1738–1742.
22. Iida H, Ruotsalainen U, Mäki M, et al. F-18 fluorodeoxyglucose uptake and water-perfusable tissue fraction in assessment of myocardial viability. *Ann Nucl Med.* 2012;26:644–655.
23. Knaapen P, Boellaard R, Götte MJW, et al. Perfusable tissue index as a potential marker of fibrosis in patients with idiopathic dilated cardiomyopathy. *J Nucl Med.* 2004;45:1299–1304.
24. Kajander SA, Joutsiniemi E, Saraste M, et al. Clinical value of absolute quantification of myocardial perfusion with ^{15}O-water in coronary artery disease. *Circ Cardiovasc Imaging.* 2011;4:678–684.

25. Maaniitty T, Stenström I, Saraste A, Knuuti J. Extensive and balanced reduction of myocardial blood flow in patients with suspected obstructive coronary artery disease: ^{15}O-water PET study. *Int J Cardiol.* 2021;338:1–7.
26. Maaniitty T, Knuuti J, Saraste A. ^{15}O-water PET MPI: current status and future perspectives. *Semin Nucl Med.* 2020;50:238–247.
27. Nammas W, Maaniitty T, Knuuti J, Saraste A. Cardiac perfusion by positron emission tomography. *Clin Physiol Funct Imaging.* 2021;41:385–400.
28. Rehan R, Yong A, Ng M, Weaver J, Puranik R. Coronary microvascular dysfunction: a review of recent progress and clinical implications. *Front Cardiovasc Med.* 2023;10:1111721.
29. Bhatt DL, Gabriel Steg P, Magnus Ohman E, et al. International prevalence, recognition, and treatment of cardiovascular risk factors in outpatients with atherothrombosis. *JAMA.* 2006;295:180–189.
30. Crea F, Camici PG, Merz CNB. Coronary microvascular dysfunction: an update. *Eur Heart J.* 2014;35:1101–1111.
31. Swirski FK, Nahrendorf M. Cardioimmunology: the immune system in cardiac homeostasis and disease. *Nat Rev Immunol.* 2018;18:733–744.
32. McDonagh TA, Metra M, Adamo M, et al. 2021 ESC guidelines for the diagnosis and treatment of acute and chronic heart failure. *Eur Heart J.* 2021;42:3599–3726.
33. Zannad F, Rossignol P. Cardiorenal syndrome revisited. *Circulation.* 2018;138: 929–944.
34. Peterson LR, Gropler RJ. Metabolic and molecular imaging of the diabetic cardiomyopathy. *Circ Res.* 2020;126:1628–1645.
35. Tahsili-Fahadan P, Geocadin RG. Heart–brain axis. *Circ Res.* 2017;120:559–572.
36. Knuuti J, Wijns W, Saraste A, et al. 2019 ESC guidelines for the diagnosis and management of chronic coronary syndromes: the task force for the diagnosis and management of chronic coronary syndromes of the European Society of Cardiology (ESC). *Eur Heart J.* 2020;41:407–477.
37. Smith EE, Saposnik G, Biessels GJ, et al. Prevention of stroke in patients with silent cerebrovascular disease: a scientific statement for healthcare professionals from the American Heart Association/American Stroke Association. *Stroke.* 2017; 48:e44–e71.
38. Nummenmaa L, Hari R, Hietanen JK, Glerean E. Maps of subjective feelings. *Proc Natl Acad Sci USA.* 2018;115:9198–9203.
39. Craig AD. How do you feel? Interoception: the sense of the physiological condition of the body. *Nat Rev Neurosci.* 2002;3:655–666.
40. Hare DL, Toukhsati SR, Johansson P, Jaarsma T. Depression and cardiovascular disease: a clinical review. *Eur Heart J.* 2014;35:1365–1372.
41. Hanssen TA, Nordrehaug JE, Eide GE, Bjelland I, Rokne B. Anxiety and depression after acute myocardial infarction: an 18-month follow-up study with repeated measures and comparison with a reference population. *Eur J Cardiovasc Prev Rehabil.* 2009;16:651–659.
42. Brotman DJ, Golden SH, Wittstein IS. The cardiovascular toll of stress. *Lancet.* 2007;370:1089–1100.
43. Sara JDS, Ahmad A, Toya T, Pardo LS, Lerman LO, Lerman A. Anxiety disorders are associated with coronary endothelial dysfunction in women with chest pain and nonobstructive coronary artery disease. *J Am Heart Assoc.* 2021; 10:e021722.
44. Tawakol A, Ishai A, Takx RA, et al. Relation between resting amygdalar activity and cardiovascular events: a longitudinal and cohort study. *Lancet.* 2017;389: 834–845.
45. Di Pino A, DeFronzo RA. Insulin resistance and atherosclerosis: implications for insulin-sensitizing agents. *Endocr Rev.* 2019;40:1447–1467.
46. Rask-Madsen C, King GL. Vascular complications of diabetes: mechanisms of injury and protective factors. *Cell Metab.* 2013;17:20–33.
47. Muniyappa R, Iantorno M, Quon MJ. An integrated view of insulin resistance and endothelial dysfunction. *Endocrinol Metab Clin North Am.* 2008;37:685–711.
48. Barrett EJ, Rattigan S. Muscle perfusion: its measurement and role in metabolic regulation. *Diabetes.* 2012;61:2661–2668.
49. Jochumsen MR, Overgaard DL, Vendelbo MH, et al. Extracardiac findings with increased perfusion during clinical O-15-H_2O PET/CT myocardial perfusion imaging: a case series. *J Nucl Cardiol.* 2023;30:1458–1468.
50. Caruso M, Stanzione A, Prinster A, et al. Role of advanced imaging techniques in the evaluation of oncological therapies in patients with colorectal liver metastases. *World J Gastroenterol.* 2023;29:521–535.
51. Katayama D, Yanagawa M, Matsunaga K, et al. Greater reductions in blood flow after anti-angiogenic treatment in non-small cell lung cancer patients are associated with shorter progression-free survival. *Sci Rep.* 2021;11:6805.
52. Patel KP, Katsurada K, Zheng H. Cardiorenal syndrome: the role of neural connections between the heart and the kidneys. *Circ Res.* 2022;130:1601–1617.
53. Kero T, Saraste A, Lagerqvist B, et al. Quantitative myocardial perfusion response to adenosine and regadenoson in patients with suspected coronary artery disease. *J Nucl Cardiol.* 2022;29:24–36.
54. Schuster DP, Kaplan JD, Gauvain K, Welch MJ, Markham J. Measurement of regional pulmonary blood flow with PET. *J Nucl Med.* 1995;36:371–377.
55. van der Veldt AA, Hendrikse NH, Harms HJ, et al. Quantitative parametric perfusion images using ^{15}O-labeled water and a clinical PET/CT scanner: test-retest variability in lung cancer. *J Nucl Med.* 2010;51:1684–1690.
56. Kudomi N, Slimani L, Järvisalo MJ, et al. Non-invasive estimation of hepatic blood perfusion from H_2 ^{15}O PET images using tissue-derived arterial and portal input functions. *Eur J Nucl Med Mol Imaging.* 2008;35:1899–1911.
57. Rhodes CG, Hughes JMB. Pulmonary studies using positron emission tomography. *Eur Respir J.* 1995;8:1001–1017.
58. Ziegler SI, Haberkorn U, Byrne H, et al. Measurement of liver blood flow using oxygen-15 labelled water and dynamic positron emission tomography: limitations of model description. *Eur J Nucl Med.* 1996;23:169–177.
59. Sun T, Wu Y, Wei W, et al. Motion correction and its impact on quantification in dynamic total-body ^{18}F-fluorodeoxyglucose PET. *EJNMMI Phys.* 2022;9:62.
60. Shiyam Sundar LK, Lassen ML, Gutschmayer S, et al. Fully automated, fast motion correction of dynamic whole-body and total-body PET/CT imaging studies. *J Nucl Med.* 2023;64:1145–1153.
61. Rainio O, Han C, Teuho J, et al. Carimas: an extensive medical imaging data processing tool for research. *J Digit Imaging.* 2023;36:1885–1893.
62. Wasserthal J, Breit H-C, Meyer MT, et al. TotalSegmentator: robust segmentation of 104 anatomical structures in CT images. *Radiol Artificial Intelligence.* 2023; 5:e230024.
63. Seifert R, Herrmann K, Kleesiek J, et al. Semiautomatically quantified tumor volume using ^{68}Ga-PSMA-11 PET as a biomarker for survival in patients with advanced prostate cancer. *J Nucl Med.* 2020;61:1786–1792.
64. Bol A, Vanmelckenbeke P, Michel C, Cogneau M, Goffinet AM. Measurement of cerebral blood flow with a bolus of oxygen-15-labelled water: comparison of dynamic and integral methods. *Eur J Nucl Med.* 1990;17:234–241.
65. Wang G, Nardo L, Parikh M, et al. Total-body PET multiparametric imaging of cancer using a voxelwise strategy of compartmental modeling. *J Nucl Med.* 2022; 63:1274–1281.
66. Karjalainen T, Tuisku J, Santavirta S, et al. Magia: robust automated image processing and kinetic modeling toolbox for PET neuroinformatics. *Front Neuroinform.* 2020;14:3.
67. Rolls ET, Huang CC, Lin CP, Feng J, Joliot M. Automated anatomical labelling atlas 3. *Neuroimage.* 2020;206:116189.
68. Kudomi N, Hirano Y, Koshino K, et al. Rapid quantitative CBF and $CMRO_2$ measurements from a single PET scan with sequential administration of dual ^{15}O-labeled tracers. *J Cereb Blood Flow Metab.* 2013;33:440–448.
69. Yokoi T, Iida H, Itoh H, Kanno I. A new graphic plot analysis for cerebral blood flow and partition coefficient with iodine-123-iodoamphetamine and dynamic SPECT validation studies using oxygen-15-water and PET. *J Nucl Med.* 1993;34:498–505.
70. Iida H, Tanaka K, Hirose Y, Yamamoto S, Murakami M, Uemura K. Effect of real-time weighted integration system for rapid calculation of functional images in clinical positron emission tomography. *IEEE Trans Med Imaging.* 1995;14: 116–121.
71. Yokoi T, Kanno I, Iida H, Miura S, Uemura K. A new approach of weighted integration technique based on accumulated images using dynamic PET and $H_2{}^{15}$O. *J Cereb Blood Flow Metab.* 1991;11:492–501.
72. Wang Y, Li E, Cherry SR, Wang G. Total-body PET kinetic modeling and potential opportunities using deep learning. *PET Clin.* 2021;16:613–625.
73. Alva-Sánchez H, Zepeda-Barrios A, Díaz-Martínez VD, Murrieta-Rodríguez T, Martínez-Dávalos A, Rodríguez-Villafuerte M. Understanding the intrinsic radioactivity energy spectrum from ^{176}Lu in LYSO/LSO scintillation crystals. *Sci Rep.* 2018;8:17310.
74. Teimoorisichani M, Panin V, Rothfuss H, Sari H, Rominger A, Conti M. A CT-less approach to quantitative PET imaging using the LSO intrinsic radiation for long-axial FOV PET scanners. *Med Phys.* 2022;49:309–323.
75. Sari H, Teimoorisichani M, Mingels C, et al. Quantitative evaluation of a deep learning-based framework to generate whole-body attenuation maps using LSO background radiation in long axial FOV PET scanners. *Eur J Nucl Med Mol Imaging.* 2022;49:4490–4502.